Int. J. Heat Mass Transfer. Vol. 34, No. 6, pp. 1465–1479, 1991
Printed in Great Britain

0017–9310/91 $3.00+0.00

Critical heat flux from a simulated chip to a confined rectangular impinging jet of dielectric liquid

I. MUDAWAR and D. C. WADSWORTH

Boiling and Two-phase Flow Laboratory, School of Mechanical Engineering,
Purdue University, West Lafayette, IN 47907, U.S.A.

(*Received* 13 *February* 1990 *and in final form* 22 *June* 1990)

Abstract—Experiments are performed to investigate boiling heat transfer from a smooth 12.7 mm × 12.7 mm heat source to a jet of dielectric Fluorinert FC-72 liquid issued from a thin rectangular orifice into a channel confined between the surfaces of the heat source and the nozzle. General boiling and critical heat flux (CHF) trends are examined with respect to variations in nozzle exit velocity, $U = 1$–13 m s^{-1}, nozzle width, $W = 0.127$–0.508 mm, confinement channel height above the heated surface, $H = 0.508$–5.08 mm, and subcooling, $\Delta T_{sub} = 0$–40°C. Two regimes of CHF, medium and high velocity, are discovered, and an empirical correlation is developed for the medium velocity regime. The primary difference between the two regimes is a weak dependence of CHF on channel height for medium velocities compared to a stronger dependence for high velocities. It is found that operating in the high velocity regime, especially for the smallest channel height, can result in decreasing CHF with increasing jet velocity due to a stream-wise reduction of liquid subcooling within the channel. A self-contained cooling module consisting of a 3 × 3 array of heat sources confirms the uniformity and predictability of cooling for each of the nine heat sources, proving that the confined jet geometry is well suited for cooling large arrays of high-power-density heat sources such as electronic chips dissipating heat fluxes as high as 250 W cm^{-2}.

1. INTRODUCTION

THE HIGH heat transfer coefficients attainable with jet impingement have stimulated much research on this convective mode of heat transfer in both the past and present. This form of cooling can be found in turbine blades, X-ray medical devices, laser weapons, metallic extrusion quench chambers and textile dryers, to name a few applications. The majority of jet-impingement research has centered on single-phase heat transfer, while only a few studies (e.g. refs. [1–9]) are available on the phase-change aspects of jet impingement. Most of the existing two-phase correlations are based on data measured for water or Freon refrigerants, however, these refrigerants are currently being viewed as a threat to the environment by many organizations which are calling for a ban on their use in most household and industrial applications. Thus, a need exists for generating data bases and correlations for new types of coolants, such as the 3M dielectric Fluorinerts, which combine the attractive features of inertness and chemical compatibility with most engineering materials as well as safety to individuals and to the environment.

One application where jet impingement cooling is receiving much attention is the packaging of microelectric chips in computer systems. The current trend of miniaturization and concentration of electronic components in the chip has given rise to alarmingly high-power densities. Bar-Cohen *et al.* [10] predict future technologies may result in power densities in excess of 100 W cm^{-2} at the chip level by the mid-1990s. This problem has been compounded by a concurrent trend of reduction in the dimensions of cooling hardware aimed at reducing system size and increasing computational speed. These trends have necessitated a pursuit of higher heat transfer coefficients, a task complicated by the poor transport properties of dielectric coolants. Phase change and increased coolant velocity are two of the few means available for packaging engineers in combating the harsh cooling requirements projected for the mid-1990s. These challenging problems have triggered much research in the heat transfer community in recent years including the present study. The problem of predicting CHF for two-phase electronic cooling is important due to the potential failures which may occur at the chip and system levels as a result of local overheating of electronic components.

Several studies on CHF in jet impingement and other external forced convection boiling systems have been performed with different fluids and over wide ranges of velocity and pressure. The CHF data from these studies have commonly been reduced according to Katto's [11] correlation form

$$\frac{q_m/(\rho_g h_{fg})}{U} = f\left[\frac{\rho_g}{\rho_f}, \frac{\rho_f U^2 d}{\sigma}, \frac{g(\rho_f-\rho_g)d}{\rho_f U^2}, \frac{\mu_g}{\mu_f}, \frac{\rho_f U d}{\mu_f}\right] \quad (1)$$

where d and U are the characteristic length and characteristic velocity of the forced convection boiling system, respectively. Based on his review of experimental CHF findings, Katto suggested that the viscosity terms in equation (1) do not affect CHF, and

NOMENCLATURE

c_p	specific heat at constant pressure
C_{sub}	subcooling empirical constant
d	diameter of heated surface in circular jet studies
D	diameter of circular orifice in circular jet studies
g	acceleration due to gravity
h_{fg}	latent heat of vaporization
H	height of confinement channel
k	empirical constant
L	total length of heated surface (12.7 mm)
m	empirical constant
n	empirical constant
P	pressure
P_1	absolute pressure measured upstream of nozzle
P_2	channel outlet pressure (reference pressure for CHF data), $P_1 - \Delta P$
ΔP	pressure drop measured between nozzle upstream and channel downstream
q	heat flux based on heat source surface area
q_m	CHF
q_m^{**}	dimensionless CHF defined in equation (12)
T_f	liquid temperature upstream of nozzle
T_s	mean temperature of heated surface
T_{sat}	saturation temperature corresponding to channel outlet pressure P_2
ΔT	$T_s - T_f = \Delta T_{sat} + \Delta T_{sub}$
ΔT_{sat}	$T_s - T_{sat}$
ΔT_{sub}	$T_{sat} - T_f$
U	mean jet velocity at nozzle exit
W	width of orifice
We	Weber number, $(\rho_f U^2 L)/\sigma$
x	distance from impingement centerline.

Greek symbols

δ_m	inlet thickness of liquid sublayer
μ	dynamic viscosity
ρ	density
σ	surface tension
ψ	empirical coefficient in equation (9).

Subscripts

1	nozzle upstream condition
2	channel downstream condition
f	saturated liquid
g	saturated vapor
sat	saturated condition
sub	subcooled condition.

that gravity becomes insignificant in systems involving high flow velocities. These simplifying assumptions reduce equation (1) to the form

$$\frac{q_m/(\rho_g h_{fg})}{U} = f\left[\frac{\rho_g}{\rho_f}, \frac{\rho_f U^2 d}{\sigma}\right] \tag{2}$$

which has become a popular technique for correlating saturated CHF data.

Haramura and Katto [12] proposed a theoretical model for CHF in pool boiling and external forced convection boiling systems based upon Gaertner's [13] photographic investigation of pool boiling. The model was based upon the hypothesis that, prior to CHF, vapor accumulates on the heated surface in the form of large bubbles due to Helmholtz instability of the vapor jets issuing normal to the surface. Gaertner's observation on the existence of a thin liquid sublayer beneath the large coalescent vapor bubbles was suggested by Haramura and Katto to be the primary source of cooling for the surface prior to CHF in pool boiling as well as external forced convection boiling systems. They also suggested CHF occurs when liquid inflow from the bulk liquid to the sublayer becomes insufficient in balancing the rate of sublayer evaporation.

The Haramura and Katto model was modified in ref. [14] to take into account the effect of bulk liquid subcooling in the boiling of a liquid film flowing over a heated surface. The modified model accounts for the effect of liquid subcooling on both the Helmholtz instability of the vapor jets issuing normal to the heated surface and on the additional sensible energy the heated surface has to overcome as the subcooled liquid enters the sublayer near the upstream region of the heated surface. The ratio of subcooled to saturated CHF was presented as

$$\frac{q_{m,sub}}{q_m} = \left[1 + \frac{c_{pf}\Delta T_{sub}}{h_{fg}}\right]^{1/3}\left[1 + C_{sub}\frac{\rho_f c_{pf}\Delta T_{sub}}{\rho_g h_{fg}}\right]^{2/3} \tag{3}$$

where C_{sub} is an empirical constant.

The new subcooled CHF model was also successful at correlating the data of ref. [15] for CHF from a small heat source flush-mounted to the wall of a rectangular flow channel. Both the falling liquid film and channel flow studies included flow visualization experiments which demonstrated the existence of the thin liquid sublayer prior to CHF as well as the ensuing dryout following CHF. However, the channel flow experiment revealed the existence of two distinct mechanisms for CHF. At low flow velocities, CHF occurred after a single vapor blanket formed over the entire heated surface, allowing liquid inflow only from the upstream region of the sublayer. The rapid temperature rise associated with CHF followed dryout of

the sublayer. At high velocities, several small discrete vapor blankets formed on the surface and sublayer dryout occurred beneath the discrete blankets. Data in the high velocity range did not follow the trends predicted by the Katto and Haramura model or the modified model.

The existence of different CHF mechanisms for different velocity ranges was also mentioned by Monde [8] in his investigation of CHF from a heated surface to a jet impinging normal to the surface from a circular orifice. Originally, Monde introduced a generalized correlation for circular jet CHF data which he based upon data measured by Katto and Kunihiro [2], Monde and Katto [3, 5], Katsuta [4], Katto and Shimizu [6], and Monde [7]

$$\frac{q_m/(\rho_g h_{fg})}{U} = 0.221\left[\frac{\rho_f}{\rho_g}\right]^{0.645}\left[\frac{2\sigma}{\rho_f U^2(d-D)}\right]^{0.343}\left[1+\frac{d}{D}\right]^{-0.364} \quad (4)$$

where d and D are the diameters of the heated surface and the nozzle orifice, respectively. Equation (4) was determined from the theoretical arguments of Katto and Haramura except for small perturbations in the exponents 0.343 and -0.364 which were predicted as $1/3$ and $-1/3$ according to the theoretical model. Monde's generalized correlation suggests that the inverse Weber number be based upon the heated region over which sublayer dryout occurs and that equation (4) be modified with a dimensionless geometrical term where the boiling system has more than one characteristic length.

Recently, Monde [9] indicated equation (4) is not necessarily valid for all flow conditions even when corrected with a dimensionless geometrical term. For example, he suggested the gravity term in equation (1) can become important for jet impingement at low velocity onto a downward-facing heated surface with a large d/D ratio. Thus, he identified different CHF regimes (the V-, L-, I- and HP-regimes), recommending a different correlation for each regime. Excluding the gravity-dependent L-regime, he proposed the relation

$$\frac{q_m/(\rho_g h_{fg})}{U} = C\left[\frac{\rho_f}{\rho_g}\right]^m\left[\frac{2\sigma}{\rho_f U^2(d-D)}\right]^n\left[1+\frac{d}{D}\right]^k \quad (5)$$

for correlating data associated with each of the three other flow regimes. The significant differences between the empirical constants m, n and k correlated by Monde for each regime suggest marked differences in the CHF mechanism at different operating conditions, an important conclusion also reached in ref. [15].

This study addresses the boiling and CHF phenomena associated with a rectangular jet impinging onto a 12.7 mm × 12.7 mm heat source. The paper examines phenomenological heat transfer problems created by practical considerations in the design of computers, turbine blades, X-ray medical devices and laser weapons. The need to reduce the size of cooling hardware is investigated by examining the effect of confining the flow downstream from the impingement zone within a channel formed between the heated surface and the opposite nozzle plate. The effect of confinement on CHF is examined with respect to variations in jet velocity, jet width, confinement channel height and subcooling, and an empirical correlation is presented for CHF corresponding to moderate jet velocities. Also addressed is the issue of packaging the jet-impingement hardware in a modular arrangement capable of uniformly cooling large arrays of discrete heat sources.

2. EXPERIMENTAL METHODS

Coolant FC-72, a product of 3M, was utilized in the present experiments since its atmospheric pressure boiling point of 56°C makes it well suited for two-phase cooling of most types of electronic hardware. Information concerning the chemistry and thermophysical properties of this fluid can be found in the appendix of ref. [15].

In order to investigate jet-impingement heat transfer at the chip (heat source) and module (multi-heat source) levels, a cooling module, capable of uniformly supplying coolant to, and rejecting it from a single chip or an array of chips, was needed. The cooling module was designed to accommodate a 3 × 3 array of 12.7 mm × 12.7 mm chips. The coolant was supplied independently to each of the nine chips via a single isolated rectangular slot centered with respect to each chip. As shown in Fig. 1, the module consisted of four parallel attachments: a front cover plate, a cooling block, an electronic component (heat source) plate, and a back cover. Fiberglass composite G-10 was used for the construction of the front cover plate and the cooling block while another high-temperature fiberglass composite, G-7, was used for fabricating the electronic component plate and the back cover.

Fluid was introduced into the module through an inlet in the front cover plate. A flow deflector downstream from the inlet helped create uniform pressure in the chamber formed between the front cover plate and the cooling block. The flow was then distributed among the nine nozzles, from which fluid impinged onto the oxygen-free copper surfaces of the chips which were flush-mounted in the electronic component plate. Following impingement, the flow was confined in a channel formed between the surfaces of the nozzle and the chip. After exiting the channel, the fluid was routed vertically upward to the cooling module outlet. The module was designed to ensure cooling uniformity among the chips by producing a total pressure drop across the nozzle and the confinement channel significantly larger than the pressure drop in the upstream chamber and outlet regions.

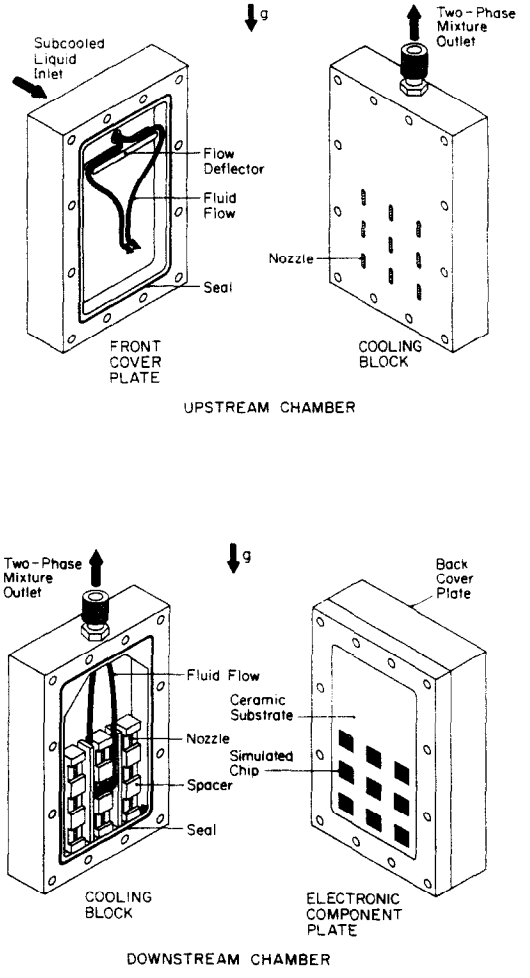

FIG. 1. Cooling module.

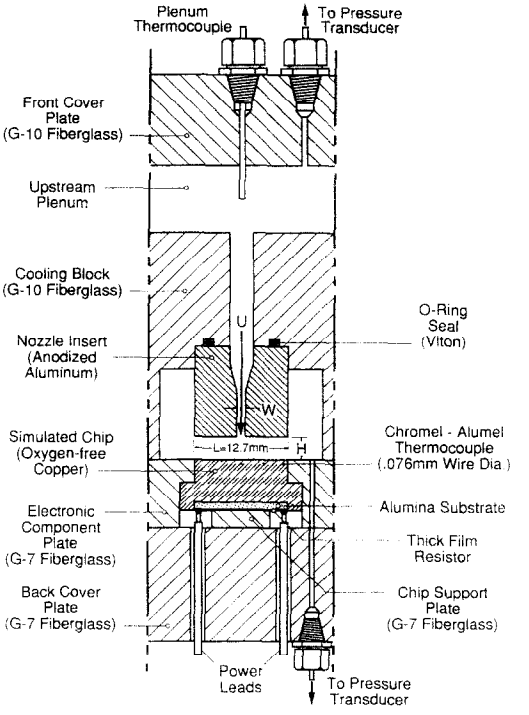

FIG. 2. Sectional diagram of cooling module.

Figure 2 shows a detailed sectional view of the cooling module. A type-K (chromel–alumel) thermocouple was inserted through the front cover and into the inlet chamber for measurement of the liquid inlet temperature. Jet inlet pressure was measured by a pressure transducer connected to the inlet chamber. A differential pressure transducer connected between the inlet chamber and confinement channel outlet measured the total pressure drop across the nozzle and the confinement channel.

The geometrical parameters of the impinging flow were set by using different nozzle inserts which were recessed into the G-109 cooling block. The anodized aluminum nozzle inserts consisted of a 30° converging entrance region followed by a straightening section five times the jet width.

A thick-film resistor was used to provide heat to the chip surface. The resistor was deposited on one side of an alumina substrate, which was solder-coated on the backside for convenient bonding to the oxygen-free copper block. The solder coating also served to eliminate contact resistances between the heating element and the copper block.

The copper boiling surface was blasted with a slurry of air/water/silica at high pressure (100 psi), creating a homogeneous and consistent microstructure having an effective pore diameter of approximately 15 μm [16]. Three type-K thermocouples measured the chip temperature. Each thermocouple was constructed from 0.127 mm (0.005 in.) wire and insulated with a two-hole ceramic tube. The thermocouple beads were coated with a thermally-conducting epoxy containing boron nitride powder to prevent direct contact between the beads and the copper while ensuring quick temperature response. The thermocouple assemblies were inserted into 0.794 mm (0.031 in.) holes in the copper block in planes parallel to the chip surface. One thermocouple was placed along the centerline of the chip corresponding to the impingement zone and the other two were distributed parallel to the flow direction.

A worst-case heat loss was estimated numerically by assuming zero contact resistances between the heater and its mating insulating surfaces. The analysis showed a maximum heat loss of approximately 4% for the lowest values of the heat transfer coefficient in the single phase regime, and less than 1% for most boiling data. Thus, all the data presented in this paper are based on a heat flux equal to the electrical power input divided by the chip surface area. The mean surface temperature was determined, first, by correcting the temperatures measured at the thermocouple plane assuming one-dimensional conduction within the copper block normal to the heated surface and, second, by calculating an area-weighted aver-

age of the three corrected values. Within the boiling regime, the deviation between the three temperatures was typically less than 1°C, which increased to as high as 4°C just before CHF. Other details concerning measurement accuracy can be found in ref. [17].

Power to the thick-film resistors was supplied by a 240 Vac variac and measured using voltage and current transducers which converted the a.c. voltage and current signals to d.c. signals conditioned for the data acquisition system. Signals from the current and voltage transducers, pressure transducers, and thermocouples were monitored and recorded using a Keithley series-500 data acquisition system and processed by a Compaq 286 microcomputer. Other features of the data acquisition system included taking and plotting data simultaneously, shutting off the power supplied to a given heater automatically as the heater encountered CHF, and controlling pressure via a solenoid valve connected in the water supply line of the main condenser in the flow loop.

2.1. *Operating procedure*

The operating procedure for each run consisted of deaerating the coolant by energizing the module test heaters and several immersion heaters in the flow loop while circulating the fluid through the system. Figure 3 shows the flow loop. During deaeration, pressure in the module was held at approximately 1.3 atm and the fluid temperature was raised to 60°C, the saturation temperature of FC-72 corresponding to the same pressure. The deaeration process continued for approximately 20 min during which time air and FC-72 vapor were being released from the loop into a condensate tank. Following deaeration, the system was isolated from the ambient by closing off the system outlet to the condensate tank.

CHF data points were acquired by incrementing the power supplied to the chip in a step-wise fashion and waiting for steady-state conditions between increments. Steady state was determined after the standard deviation of 20 fluid and surface temperature readings taken over a 40 s time period was less than or equal to 0.15°C. CHF typically occurred when the chip surface temperature neared 100°C; therefore, as the surface temperature approached 100°C, the power increments were reduced to approximately 1 W m^{-2}. The CHF was defined as the last steady-state flux value above which a small increment in power triggered a sharp increase in temperature. In this manner, the CHF point was identified to within 1 W m^{-2}, 4% for the worst case and approximately 1% for the majority of tests. During the sharp temperature excursion following CHF, the surface temperature would exceed a preset value, generally 120°C, at which point the data acquisition system would automatically cut

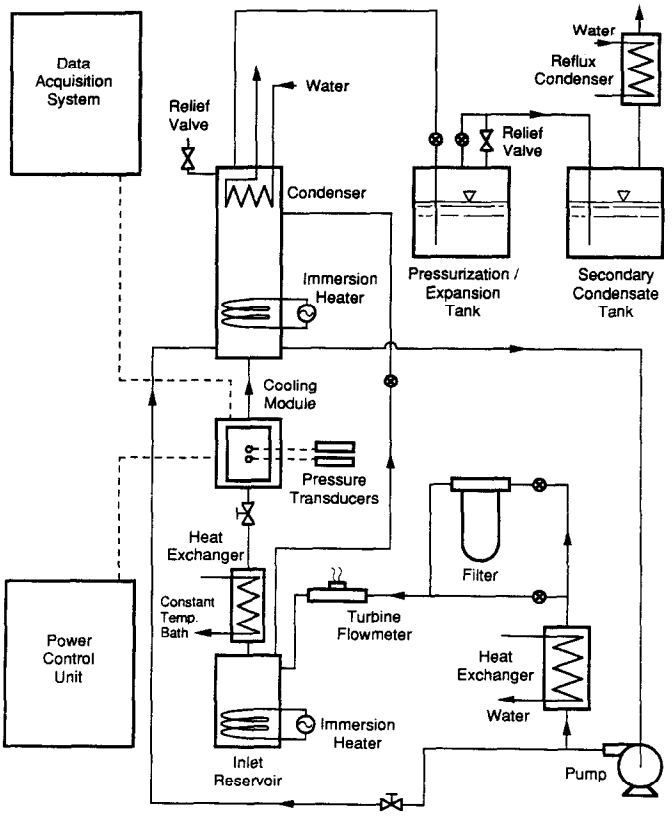

FIG. 3. Schematic diagram of flow loop.

Table 1. CHF experimental test matrix

Nozzle width, W	Degree of subcooling, ΔT_{sub} (°C) Nozzle height, H 0.508 mm (0.020 in.)	1.27 mm (0.050 in.)	2.54 mm (0.100 in.)	5.08 mm (0.200 in.)
0.127 mm (0.005 in.)	10	0, 10, 20, 30, 40	10	0, 10, 20, 30, 40
0.254 mm (0.010 in.)	10	10	10	10
0.381 mm (0.015 in.)	10	0, 10	10	0, 10
0.508 mm (0.020 in.)	10	10	10	10

$1 < U < 13$ m s^{-1}, $1.2 < P < 1.6$ bar

off the power supplied to the heater to prevent potential damage to the thick-film resistor. This power control mechanism enabled heaters to endure several CHF tests.

3. RESULTS AND DISCUSSION

It was difficult to operate the system at or near the saturation temperature of FC-72 without inducing flashing because of the pressure drop across the nozzle. The practical minimum limit on fluid subcooling for many of the 'saturated' CHF data was about 4°C. For consistency, it was decided that the bulk of the CHF reference data be taken with $\Delta T_{sub} = 10.0 \pm 0.15$°C, a condition which could easily be maintained in the flow loop. The parametric trends of CHF were examined with respect to variations in jet velocity, $U = 1$–13 m s^{-1}, jet width, $W = 0.127$–0.508 mm, confinement channel height, $H = 0.508$–5.08 mm, and subcooling, $\Delta T_{max} \cong 0$–40°C. Sixteen nozzle inserts were machined for each vertical three-chip column, Fig. 1, providing the necessary variations in W and H for the entire module. Sixteen additional inserts provided similar variations in H and W for the central chip alone while the flow through nozzles facing the other eight chips was being blocked. These latter inserts facilitated the generation of a CHF reference data base corresponding to the central chip. A complete matrix of the operating conditions is provided in Table 1.

Figures 4 and 5 show the effects of impingement velocity and fluid subcooling, respectively, in the form of boiling curves plotted with respect to $(T_s - T_f)$ instead of $(T_s - T_{sat})$. The advantage of the former is that it facilitates a useful representation of single-phase data for subcooled boiling conditions. Saturation conditions for the boiling and CHF data were references with respect to the channel outlet pressure due to the small ratio of pressure drop across the channel to total pressure drop across the jet and the channel. This approximation was confirmed by the observation that the total pressure drop measured for

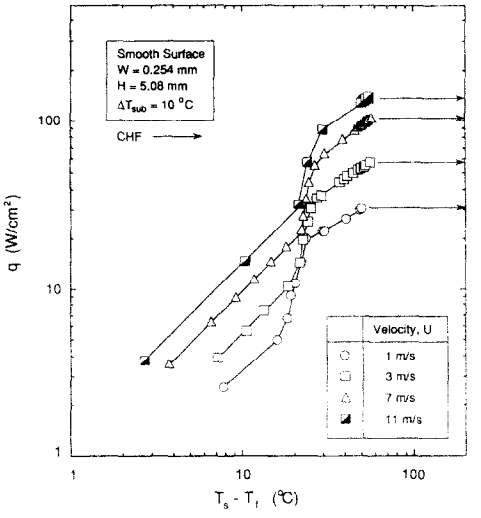

FIG. 4. Effect of impingement velocity on the boiling curve.

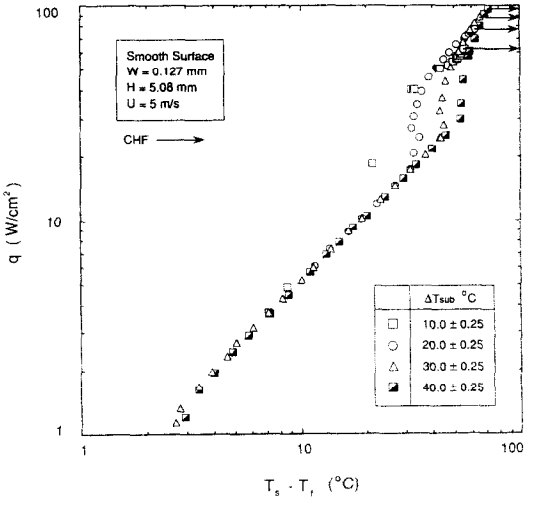

FIG. 5. Effect of fluid subcooling on the boiling curve.

a given nozzle width was fairly constant as H was decreased from 5.08 to 0.508 mm. This issue will be discussed in more detail later in this section.

Velocity, as depicted in Fig. 4, had a pronounced effect on all the heat transfer regimes of the boiling curve. Increasing velocity augmented the single-phase heat transfer considerably and delayed the point of boiling incipience to a higher heat flux and a higher surface temperature. For all velocities examined, the nucleate boiling data seemed to fall onto a single line, a phenomenon previously demonstrated by McAdams *et al.* [18], and Bergles and Rohsenow [19]. Perhaps the most significant feature of Fig. 4 is a CHF enhancement in excess of 300% obtained by increasing velocity from 1 to 11 m s^{-1}.

Figure 5 shows the influence of fluid subcooling on the boiling curve. In the single-phase regime, the convective heat transfer coefficient was affected slightly by the variations of coolant properties with temperature. There was a noticeable effect of subcooling on the point of incipience. The heat flux and surface temperature corresponding to incipience both increased with increasing subcooling. Figure 5 also shows a significant enhancement in CHF due to subcooling.

Figures 6 and 7 display variations of CHF with impingement velocity for a representative portion of the 16 nozzle configurations and 10°C subcooling. Figures 6(a) and (b) show that, for a constant nozzle width, channel height has a weak effect on CHF in the medium velocity range of about 1.5–7 m s^{-1}, and a marked effect at higher velocities. Figures 7(a) and (b) demonstrate that CHF increases in the medium velocity range with increasing jet width.

Data in Figs. 6 and 7 suggest the existence of two distinct CHF regimes. The dependence of CHF on velocity in the medium velocity regime may be approximated as $q_m \propto U^{0.7}$. The high velocity regime is characterized by a leveling off of CHF, followed by a decrease in CHF with increasing velocity. As shown, the transition from the medium to the high velocity regime is related to the channel height. The transition occurred at lower velocities as the channel height was decreased, indicating an increase in void ratio in the two-phase flow within the confinement channel for small values of H. The medium and high velocity regimes were also identifiable in the data taken near saturation conditions. For a given geometrical configuration, the transition commenced at a lower velocity for saturated compared to subcooled flow. For example, with $W = 0.381$ mm and $H = 1.27$ mm, the transition occurred at a velocity between 9 and 11 m s^{-1} for $\Delta T_{sub} = 10$°C compared to a velocity between 5 and 7 m s^{-1} for $\Delta T_{sub} \cong 4.8$°C. This difference could also be due to the increased void ratio associated with boiling near saturated conditions.

Figure 8 shows the influence of subcooling on CHF in the medium velocity regime for $W = 0.127$ mm and $H = 1.27$ mm. Increasing the fluid subcooling from approximately 4.5 to 10°C increased CHF nearly

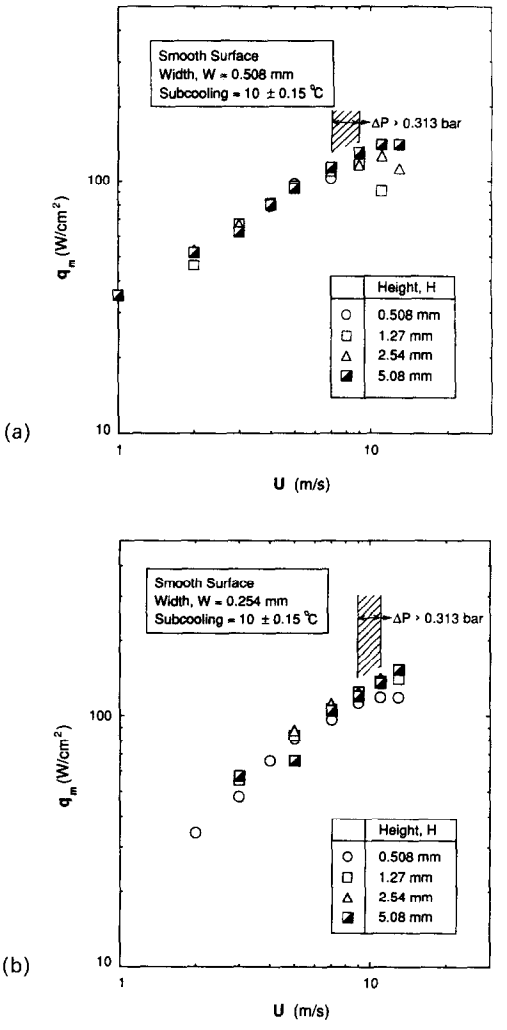

FIG. 6. Variation of CHF with velocity corresponding to four confinement channel heights for: (a) $W = 0.508$ mm; (b) $W = 0.254$ mm.

30%. As the fluid subcooling was increased to 40°C, CHF was enhanced 130% compared to the near saturated condition. Thus, subcooling offers at least two advantages to the confined-jet cooling scheme: delaying the onset of the high velocity regime where CHF eventually decreases with increasing coolant flow rate and increasing the CHF value, all other parameters being held constant. The highest CHF value attained in the present study was 249 W cm^{-2} corresponding to $W = 0.508$ mm, $H = 5.08$ mm, $U = 12.9$ m s^{-1} and $\Delta T_{sub} = 40$°C.

The point of transition between the medium and high velocity regimes should be considered as an upper design limit since, for a given geometrical configuration, operation at velocities exceeding this point can result in an adverse relationship between coolant flow rate and CHF.

3.1. *Uncertainty in the determination of local pressure and subcooling*

In comparing CHF data obtained from different tests, it is important that the conditions for these

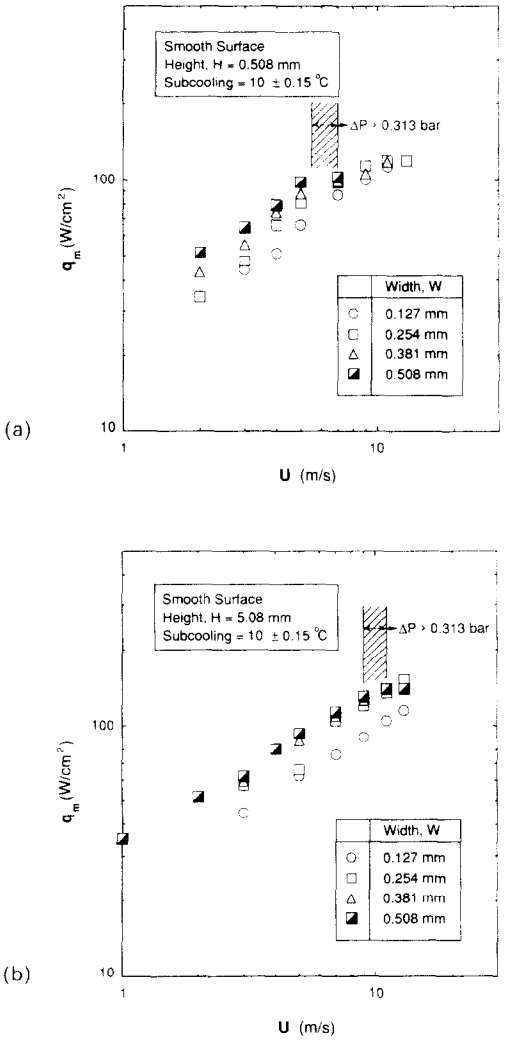

FIG. 7. Variation of CHF with velocity corresponding to four nozzle widths for: (a) $H = 0.508$ mm; (b) $H = 5.08$ mm.

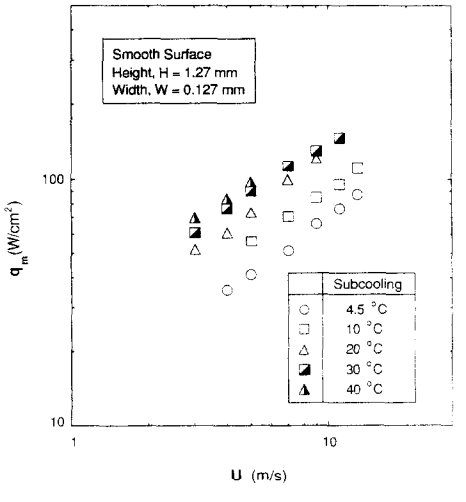

FIG. 8. Effect of fluid subcooling on the variation of CHF with jet velocity for $W = 0.127$ mm and $H = 1.27$ mm.

tests be referenced to common operating pressures. As mentioned before, the saturation pressure within the channel was assumed equal to the channel outlet pressure because the total pressure drop measured between the nozzle upstream and channel downstream for a fixed jet width and fixed velocity changed very slightly with decreasing channel height. Table 2 shows representative pressure measurements for $W = 0.508$ mm, $\Delta T_{sub} = 10$ C, four channel heights and seven jet velocities. P_1 is the pressure measured upstream of the nozzle, ΔP the differential pressure drop measured across the jet and channel, and P_2 the pressure just downstream from the channel, which was used to determine saturation properties in the correlation of CHF data. The entire data base was obtained for a fairly uniform channel downstream pressure P_2. In order to minimize the error in comparing CHF data from different tests, it is important to determine whether the pressure within the channel was indeed fairly constant and equal to P_2 since pressure changes affect the saturation conditions and fluid properties.

The change in saturation temperature can be related to the change in channel pressure by the Clausius Clapeyron relation

$$\delta T_{sat} \cong \frac{T_{sat} v_{fg}}{h_{fg}} \delta P_{sat}. \tag{6}$$

Using saturation properties calculated at a mean pressure of 1.41 bar ($T_{sat} = 340.2$ K) and assuming $\delta P_{sat} < 0.5\Delta P$ gives $\Delta P < 0.313$ bar for $\delta T_{sat} < 3.5$ C. Values of ΔP exceeding 0.313 bar are identified in bold print in Table 2. These values correspond to velocities in excess of 7 m s^{-1} for 1.27 mm $\leqslant H \leqslant$ 5.08 mm and ~ 5 m s^{-1} for $H = 0.508$ mm, and correspond to the high velocity CHF regime as indicated in Figs. 6 and 7. Table 2 shows that for fixed nozzle width and jet velocity, the total pressure drop was insensitive to changes in channel height for 1.27 mm $< H <$ 5.08 mm, but increased for $H = 0.508$ mm. Furthermore, for fixed nozzle width and channel height, ΔP increased significantly with increasing jet velocity, producing large changes in saturation conditions and fluid properties. Hence, the high ΔP regions indicated in Figs. 6 and 7 are regions of relatively large uncertainty in the correlation of CHF data.

The second issue in defining reference conditions for the CHF data is to determine whether ΔT_{sub} is indeed equal to the saturation temperature based on P_2 minus the liquid temperature upstream of the nozzle. This issue requires a close examination of the changes in bulk liquid temperature and pressure between the nozzle upstream and channel downstream.

It is well known from single-phase studies on *free* rectangular jets that both the jet velocity and the ratio H/W have strong effects on the variation of pressure along the impingement surface [20]. Figure 9 shows the flow from the nozzle orifice maintaining a poten-

Table 2. Pressure measurements and corresponding reference saturation pressure at CHF for $W = 0.508$ mm and $\Delta T_{sub} = 10°C$

H (mm)		U (m s^{-1}) 3	4	5	7	9	11	13
0.508	P_1	1.321	1.355	1.427	1.686	—	—	—
	ΔP	0.081	0.120	0.185	**0.322**	—	—	—
	P_2	1.240	1.235	1.242	1.364	—	—	—
1.27	P_1	1.284	1.313	1.346	1.444	1.641	1.869	—
	ΔP	0.042	0.069	0.110	0.207	**0.327**	**0.549**	—
	P_2	1.242	1.244	1.236	1.237	1.314	1.320	—
2.54	P_1	1.304	1.338	1.374	1.477	1.665	1.884	2.270
	ΔP	0.065	0.097	0.133	0.234	**0.355**	**0.575**	**0.958**
	P_2	1.239	1.241	1.241	1.243	1.310	1.309	1.312
5.08	P_1	1.290	1.320	1.360	1.484	1.701	1.926	2.290
	ΔP	0.051	0.079	0.121	0.243	**0.398**	**0.625**	**0.999**
	P_2	1.239	1.241	1.239	1.241	1.303	1.301	1.291

$W = 0.508$ mm, $\Delta T_{sub} = 10°C$.

P_1, absolute pressure measured upstream of nozzle (bar).

ΔP, total pressure drop measured between nozzle upstream and channel downstream (bar).

P_2, reference pressure for CHF data $= P_1 - \Delta P$ (bar).

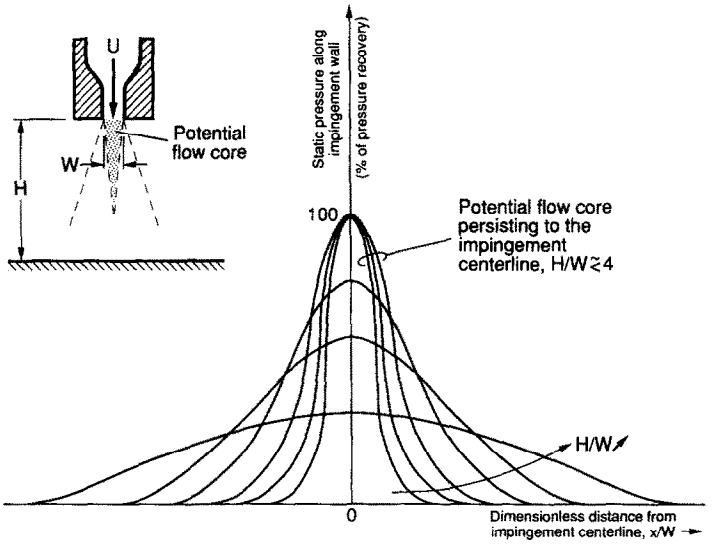

FIG. 9. Effect of H/W on the pressure distribution along the impingement surface of an unconfined jet (after Gardon and Akfirat [20]).

tial core unaffected by entrainment from, and mixing with, the fluid surrounding the jet. For small values of H/W the potential core persists to the impingement centerline, producing full recovery of the dynamic head upon impingement, followed by a decrease in pressure to the ambient level over a short distance from the centerline. Increasing H/W enhances the entrainment and, eventually, brings about full mixing of the potential core with the ambient fluid, resulting in a significant reduction in pressure recovery at the impingement centerline.

Marked differences can also be expected between the performances of *confined* jets with high versus those with low H/W values. Jets with $H/W \lesssim 1$ recover most of their dynamic head along the impingement centerline and force the flow into a channel having a relatively small hydraulic diameter. Along such a channel both the pressure drop and liquid temperature increase drastically. On the other hand, jets with $H/W \gg 1$ recover a small percentage of their dynamic head and produce a wall jet attached to the impingement wall which is unaffected by variations in H/W. This latter case produces a fairly uniform pressure in the channel equal to P_2. In a previous study by the authors [17], flow visualization with pure liquid helped demonstrate that the streamlines of liquid leaving the nozzle tend to remain close to the heated surface unaffected by the presence of the opposite confining surface of the nozzle. Furthermore, an extensive single-phase heat transfer data base for

geometrical and flow conditions similar to those of the present study showed that the heat transfer coefficient was independent of H.

Since pressure drop across the channel for $H/W \gg 1$ is smaller than the dynamic head of the jet, a simple criterion for checking whether T_{sat} is fairly uniform within the channel can be written as

$$\frac{T_{sat} v_{fg}}{h_{fg}} \frac{1}{2} \rho_f U^2 < \max |\delta T_{sat}| \quad (7)$$

where $\max |\delta T_{sat}|$ is the maximum allowable deviation in T_{sat}. Of course, this criterion is of little value for cases with small H/W due to the additional pressure drop associated with the channel for these cases.

The two extreme cases of very large and very small H/W are shown schematically in Fig. 10 in relation to the P–T saturation curve for identical reference values of T_1 and P_2. A relatively small change in ΔT_{sub} is shown for the large H/W case compared to a large stream-wise reduction in ΔT_{sub} for $H/W \cong 1$. In other words, liquid in a system with a small H/W tends to be less subcooled and, consequently, produces smaller CHF values, which is indeed the trend displayed in Figs. 6 and 7. It is important to note that these trends can be complicated by the additional pressure drop within the nozzle throat and the phase change occurring within the channel. Near CHF, a smaller H/W might increase the frictional and accelerational components of pressure drop drastically.

The present results indicate that single-phase transport plays a vital role in determining the local thermodynamic conditions of the fluid. Except for tests performed with a channel height of 0.508 mm, increasing the heat flux in a given test (including near saturated conditions) between the single-phase region and CHF resulted in a negligible change in the total pressure drop. This is evidence of a suppression of the volumetric rate of vapor production within the channel caused, in part, by the small departure size of bubbles for $U \gtrsim 2$ m s^{-1} as was indeed demonstrated photographically in ref. [15].

To better understand the effect of subcooling on CHF, it is also important to examine the mechanism of bulk liquid interaction with the wall during vigorous boiling. At very high velocities, the bulk liquid flows in the form of a wall jet strongly attached to the heated surface. High velocities also produce high single-phase heat transfer coefficients and reduce bubble size, which, in turn, confine the interaction of the bulk liquid with the wall to a thin layer of the wall jet. This increases the temperature of the portion of the bulk liquid mass flow which affects the boiling process. Consequently, the effectiveness of liquid subcooling can be greatly diminished in the stream-wise direction. In contrast, low velocities produce wall jets which are not as strongly attached to the heated wall. Also, the relatively large bubble size at low velocities induces bulk liquid further away from the wall to lose its sensible energy and/or evaporate at the wall. This results in a relatively large fraction of liquid mass flow interacting with the wall. Therefore, the bulk liquid subcooling available for CHF enhancement is greatly reduced at high flow velocities compared to low velocities as is clearly shown in Figs. 6 and 7.

3.2. *CHF correlation*

By comparing flow velocities of the present study to those of ref. [15] for flow parallel to a small heated surface, it becomes apparent that the medium velocity range of the present study, $U \cong 1.5$–7 m s^{-1}, is beyond the so-called low velocity range identified in the parallel flow study, $U \leqslant 2$ m s^{-1}, for which the mechanism of sublayer dryout over the entire surface has been validated as a precursor for CHF. It was shown [15] that parallel flow velocity exceeding the low velocity range, and within the medium velocity range of the present study, resulted in a different CHF mechanism consisting of the random formation of small, discrete vapor blankets over the heated surface and dryout of liquid sublayers at CHF beneath the individual blankets. These two regimes are represented

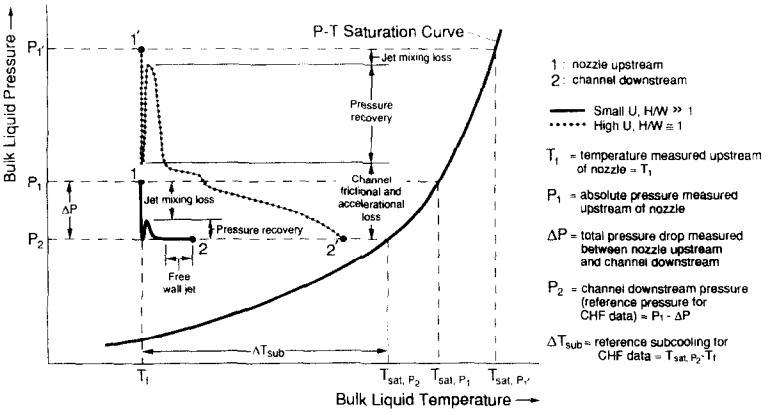

FIG. 10. Effects of U and H/W on the pressure and temperature variations of the portion of bulk liquid mass flow undergoing sensible and/or latent heat exchange with the heated wall between the nozzle upstream and channel downstream.

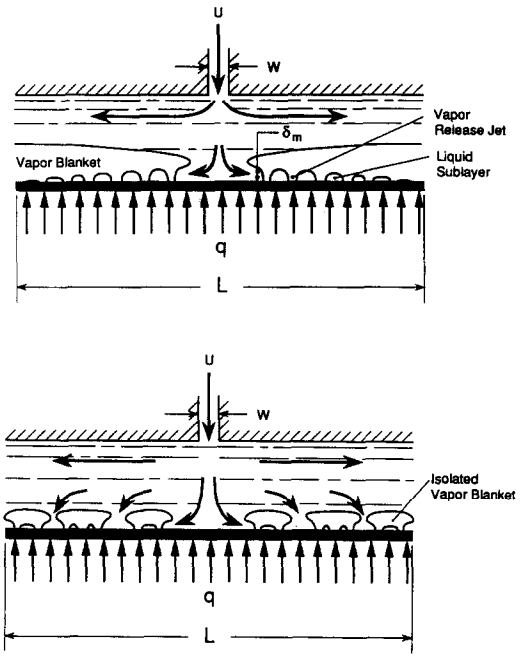

FIG. 11. CHF sublayer dryout mechanisms for: (a) the low velocity regime (below the velocity range of the present study); (b) the medium velocity regime.

schematically in Figs. 11(a) and (b) for the confined-jet geometry. Figure 11(a) is based upon the jet impingement studies by Katto and Monde [3], and the photographic studies of ref. [14] on CHF in falling films and of ref. [15] on CHF in channel flow parallel to a small heated surface. CHF in all the three studies was preceded by separation of the main liquid flow away from the surface by a vapor blanket which covered the entire surface except for a thin liquid sublayer which maintained contact with the surface as it was being nourished by liquid inflow from upstream. CHF was accompanied by dryout of the sublayer as the upstream liquid inflow was no longer capable of balancing the rate of sublayer mass loss by evaporation.

Figure 11(a) shows the CHF condition can be determined from a balance between the sensible plus latent heat of liquid entering the sublayer and the power dissipated by the heater over the surface area undergoing sublayer evaporation

$$q_m\left[\frac{L-W}{2}\right]=\rho_f U\delta_m(h_{fg}+c_{pf}\Delta T_{sub}) \qquad (8)$$

where δ_m is the sublayer upstream thickness determined from the Helmholtz criterion given in ref. [14]

$$\delta_m=\psi\left[\frac{\sigma}{\rho_g\left(\frac{q_m}{\rho_g h_{fg}}\right)^2}\right]\left[1+C_{sub}\frac{\rho_f c_{pf}\Delta T_{sub}}{\rho_g h_{fg}}\right]^2 \qquad (9)$$

ψ being a fairly constant coefficient for $\rho_g/\rho_f \ll 1$.

Combining equations (8) and (9) yields the following expression for CHF:

$$\frac{\left[\frac{q_m/(\rho_g h_{fg})}{U}\right]}{\left[\frac{\rho_f}{\rho_g}\right]^{2/3}\left[1+\frac{c_{pf}\Delta T_{sub}}{h_{fg}}\right]^{1/3}\left[1+C_{sub}\frac{\rho_f c_{pf}\Delta T_{sub}}{\rho_g h_{fg}}\right]^{2/3}}=(2\psi)^{1/3}\left[\frac{\sigma}{\rho_f U^2(L-W)}\right]^{1/3} \qquad (10)$$

where the constants $(2\psi)^{1/3}$ and C_{sub} have to be determined empirically.

Upon examining equation (10) it becomes apparent that for the dryout criterion shown in Fig. 11(a) to be valid, q_m has to be proportional to $U^{1/3}$. From Figs. 6–8, the CHF for the medium velocity range of the present study varies according to $U^{0.7}$, a significant departure from the dependence predicted by equation (10). This is to be expected since equation (10) assumes dryout occurs over the entire surface area, Fig. 11(a), whereas the medium velocity CHF regime most likely corresponds to the CHF mechanism illustrated in Fig. 11(b). This latter CHF mechanism requires that the Weber number be based on a length L' instead of $L-W$, where L' is the characteristic length of a single discrete vapor blanket. Thus, the right-hand side of equation (10) should be expressed as

$$(2\psi)^{1/3}\left[\frac{\sigma}{\rho_f U^2 L'}\right]^{1/3}$$

which can only be corrected empirically in terms of known parameters in the absence of a physical model for determining the characteristic size of a discrete blanket.

To correlate the present CHF data, individual logarithmic plots of q_m vs U were generated for each set of geometrical parameters, W and H, at each of the four subcooling levels tested. Only medium velocity data corresponding to the linear portion of each plot were considered, and the data were correlated according to the relation

$$\frac{\left[\frac{q_m/(\rho_g h_{fg})}{U}\right]}{\left[\frac{\rho_f}{\rho_g}\right]^{2/3}\left[1+\frac{c_{pf}\Delta T_{sub}}{h_{fg}}\right]^{1/3}\left[1+C_{sub}\frac{\rho_f c_{pf}\Delta T_{sub}}{\rho_g h_{fg}}\right]^{2/3}}=C\left[\frac{\sigma}{\rho_f U^2(L-W)}\right]^m\left[\frac{W}{L-W}\right]^n \qquad (11)$$

which modifies equation (10) with the dimensionless geometrical term $W/(L-W)$ in accordance with Monde's [9] correlation technique (see equation (5)) for circular jets which, like the confined rectangular jet, is based upon two characteristic lengths. Equation (5) does not include a dimensionless term which accounts for the effect of channel height on CHF since

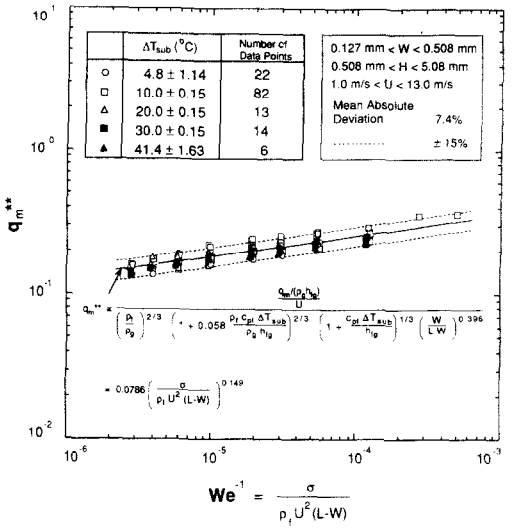

FIG. 12. CHF correlation.

this effect has been proven insignificant in the medium velocity range as shown in Fig. 6. The constants C, m, n, and C_{sub} were correlated experimentally based on a total of 137 data points as depicted in Fig. 12, resulting in the correlation

$$q_m^{**} = \left[\frac{q_m/(\rho_g h_{fg})}{U}\right] \Big/ \left\{\left[\frac{\rho_f}{\rho_g}\right]^{2/3}\left[1+\frac{c_{pf}\Delta T_{sub}}{h_{fg}}\right]^{1/3} \times \left[1+0.058\frac{\rho_f c_{pf}\Delta T_{sub}}{\rho_g h_{fg}}\right]^{2/3}\left[\frac{W}{L-W}\right]^{0.396}\right\} = 0.0786\left[\frac{\sigma}{\rho_f U^2 (L-W)}\right]^{0.149} \quad (12)$$

which fits the experimental data with a mean absolute deviation of 7.4% and a maximum deviation of 18.2%. The derivation of data from the correlation in Fig. 12 is exaggerated by a significant overlap of data points caused by operating the system at discrete values of U for a given geometrical configuration. As mentioned earlier, the exponents for the subcooling terms have been based upon the assumption of sublayer dryout illustrated in Fig. 11(b) since dryout is postulated to be the dominant mechanism for CHF in the present medium velocity data. The exponent of the density ratio term in equation (12) was fixed at 2/3 since the limited pressure range of the present data resulted in a fairly constant density ratio, $92.71 \leqslant \rho_f/\rho_g \leqslant 101.54$, which precluded an accurate correlation of the exponent.

A survey was performed of previous CHF studies involving flow over small heated surfaces to explain the unusually large value of the velocity exponent in the dependence of CHF on velocity (i.e. $q_m \sim U^{0.7}$) correlated in the present study. The studies surveyed include circular impinging jets, free plane wall jets,

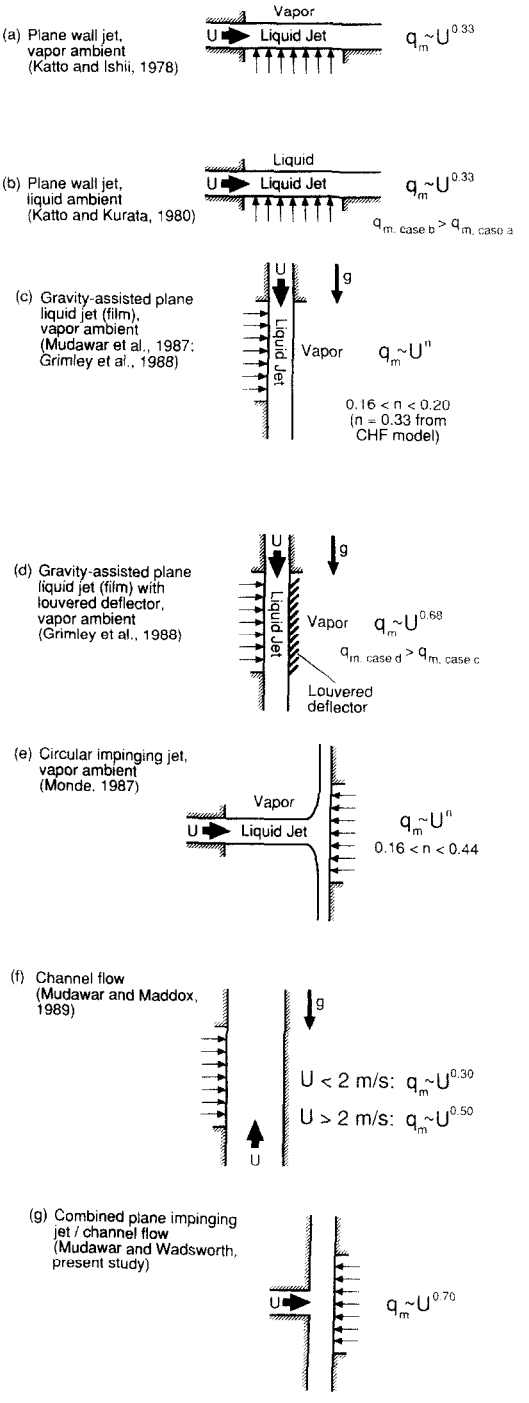

FIG. 13. CHF dependence on velocity for systems involving flow boiling on small heat sources.

confined plane wall jets and channel flow, since the present cooling configuration is a combination of jet impingement, wall jet flow and flow confinement. The dependence of CHF on velocity for each case is given in Fig. 13. All the previous correlations reveal that CHF increases with increasing flow velocity. Figure 13(f) also shows that the velocity exponent increases from a value of 0.30 for $U < 2$ m s^{-1} to 0.50 for $U > 5$

m s^{-1}. However, even for the latter high velocity range, the exponent is smaller than that of the present correlation (i.e. 0.7). By comparing the case of a gravity-assisted plane liquid jet with a deflector, Fig. 13(d), to that without the deflector, Fig. 13(c), it becomes apparent that confining the flow greatly enhances CHF and strengthens the CHF dependence on velocity. It is interesting to note that the three cases shown in Figs. 13(a)–(c) possess velocity exponents smaller than 0.33, while plane jet flow with a deflector, Fig. 13(d), shows an exponent of 0.68, almost identical to that of the present CHF correlation. As described by Grimley *et al.* [23], the use of a deflector is very effective at preventing the *bulk flow* of a plane liquid jet from separating from the heated wall during severe vapor effusion, this greatly enhancing CHF. Apparently, there exist some similarities between the enhancement effects of the confinement channel in the present study and the flow deflector in the study by Grimley *et al.* The deflection effect was insignificant in the channel flow study of ref. [15], Fig. 13(f), perhaps due to the relatively large channel height ($H = 12.7$ mm) in that particular study.

3.3. *Practical considerations*

A very important practical conclusion can be drawn from equation (12). For $W \ll L$

$$q_m \propto U^{0.702} W^{0.396} = U^{0.306}(UW)^{0.396} = \frac{(UW)^{0.702}}{W^{0.306}}. \quad (13)$$

Therefore, for a fixed coolant flow rate UW, CHF can be increased by increasing the jet velocity or by decreasing jet width. Equation (13) also indicates that, for a fixed q_m, flow rate requirements can be reduced by simply choosing a smaller jet width. For example, for the case of $W = 0.127$ mm, $H = 1.27$ mm, $U = 7$ m s^{-1} and $\Delta T_{sub} = 30°C$, a CHF value of 113.76 W cm^{-2} was achieved experimentally using a flow rate of 1.4×10^{-5} m^3 s^{-1} (0.18 gpm). By reducing jet width by a factor of two, it may be possible to reduce the flow rate to 8.39×10^{-6} (0.133 gpm) while maintaining the same CHF value. This feature, however, is limited by two practical considerations: maximum allowable pressure drop and nozzle machining/tolerance limitations.

The cooling module was tested for cooling uniformity under boiling conditions. All nine heaters were operated simultaneously under steady-state nucleate boiling conditions during which time power and temperature measurements were obtained for a fixed geometry and two jet velocities. As shown in Table 3, the temperature and heat flux measurement deviations for individual chips from mean values for the nine chips were less than 2.11%, which is approximately equal to the measurement uncertainty. This data demonstrates that the confined-jet geometry is well suited for uniformly cooling large arrays of heat sources.

4. SUMMARY

The present study examined the parametric trends of CHF from a smooth 12.7 mm × 12.7 mm chip (heat

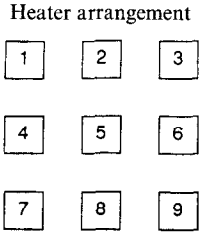

Table 3. Boiling heat transfer results for a heat source array

Heater number	$U = 0.75$ m s^{-1}				$U = 1.3$ m s^{-1}			
	ΔT (°C)		q (W cm^{-2})		ΔT (°C)		q (W cm^{-2})	
	Meas.†	% Dev.‡	Meas.†	% Dev.‡	Meas.†	% Dev.‡	Meas.†	% Dev.‡
1	21.18	−0.80	19.86	−0.05	22.26	1.04	25.08	0.32
2	21.27	−0.37	19.93	0.30	21.87	−0.73	24.81	−0.76
3	20.90	−2.11	19.84	−0.15	21.77	−1.18	25.11	0.44
4	21.63	1.31	20.90	1.11	22.31	1.27	25.05	0.20
5	21.51	0.75	19.92	0.25	22.00	−0.14	24.87	−0.52
6	21.29	−0.28	19.99	0.60	21.96	−0.32	25.15	0.60
7	21.32	−0.14	19.68	−0.96	21.90	−0.59	24.85	−0.60
8	21.47	0.56	19.73	−0.70	22.24	0.95	25.02	0.08
9	21.62	1.26	19.80	−0.35	21.98	−0.23	25.08	0.32

$W = 0.127$ mm, $H = 1.27$ mm, $\Delta T_{sub} = 10 \pm 0.15°C$.
† Meas. = measured value.
‡ % Dev. = (Measured − Mean/Mean) × 100; where Mean is the arithmetic average of the nine measured values.

source) to a two-dimensional jet of dielectric Fluorinert FC-72 liquid issued from a thin rectangular slot into a channel confined between the surfaces of the chip and the nozzle. Specific findings from the study are as follows:

(1) Two different regimes of CHF were discovered. The first corresponds to medium velocities and the second for high velocities. In the medium velocity regime, CHF increases with increasing velocity, while in the high velocity range CHF levels off and ultimately decreases with increasing velocity. Thus, the point of transition between the two regimes should be considered as an upper design limit since, for a given geometrical configuration, operation at velocities exceeding this point can result in an adverse relationship between coolant flow rate and CHF.

(2) Decreasing channel height promotes transition into the high velocity regime at lower jet velocities.

(3) The trend of decreasing CHF with increasing velocity and decreasing channel height is the result of a stream-wise reduction in liquid subcooling.

(4) CHF in the medium velocity regime increases with increasing fluid subcooling and nozzle width, but is fairly insensitive to changes in channel height.

(5) A correlation based on fluid properties, jet velocity, nozzle width, and fluid subcooling fits data in the medium velocity regime with a mean absolute deviation of 7.4%.

(6) For a given CHF, the cooling requirements of the confined-jet can be reduced by reducing the jet width.

(7) The confined-jet geometry is well suited for uniformly cooling large arrays of heat sources dissipating heat fluxes as high as 250 W cm $^{-2}$.

Acknowledgement—This material is based upon work supported by the National Science Foundation under grant No. CBT-8618949. The authors appreciate this support and thank the Industrial Chemical Products Division of 3M for providing test fluid (FC-72) for the present study.

REFERENCES

1. R. J. Copeland, Boiling heat transfer to a water jet impinging on a flat surface, Ph.D. Thesis, Southern Methodist University (1970).
2. Y. Katto and M. Kunihiro, Study of the mechanism of burnout in boiling system of high burnout heat flux, *Bull. JSME* **16**, 1357–1366 (1973).
3. Y. Katto and M. Monde, Study of mechanism of burnout in a high heat flux boiling system with an impinging jet, *Proc. 5th Int. Heat Transfer Conf.*, Tokyo, pp. 245–249 (1974).
4. M. Katsuta, Boiling heat transfer of thin liquid with an impinging jet, *Proc. 14th Natn. Heat Transfer Symp. of Japan*, pp. 154–156 (1977).
5. M. Monde and Y. Katto, Burnout in a high heat-flux boiling system with an impinging jet, *Int. J. Heat Mass Transfer* **21**, 295–305 (1978).
6. Y. Katto and M. Shimizu, Upper limit of CHF in the saturated forced convection boiling on a heated disk with a small impinging jet, *ASME J. Heat Transfer* **101**, 265–269 (1979).
7. M. Monde, Burnout heat flux in saturated forced convection boiling with an impinging jet, *Heat Transfer—Jap. Res.* **9**, 31–41 (1980).
8. M. Monde, Critical heat flux in saturated forced convection boiling on a heated disk with an impinging jet—a new generalized correlation, *Wärme- und Stoffübertr.* **19**, 205–210 (1985).
9. M. Monde, Critical heat flux in saturated forced convection boiling on a heated disk with an impinging jet, *ASME J. Heat Transfer* **109**, 991–996 (1987).
10. A. Bar-Cohen, I. Mudawar and B. Whalen, Future challenges for electronic cooling. In *Research Needs in Electronic Cooling* (Edited by F. P. Incropera), pp. 70–77. National Science Foundation and Purdue University (1986).
11. Y. Katto, Critical heat flux in forced convective flow, *Proc. ASME/JSME Thermal Engng Joint Conf.*, Hawaii, Vol. 3, pp. 1–10 (1983).
12. Y. Haramura and Y. Katto, A new hydrodynamic model of critical heat flux applicable to both pool and forced convection boiling on submerged bodies in saturated liquids, *Int. J. Heat Mass Transfer* **26**, 389–399 (1983).
13. R. F. Gaertner, Photographic study of nucleate pool boiling on a horizontal surface, *ASME J. Heat Transfer* **87**, 17–29 (1965).
14. I. Mudawar, T. A. Incropera and F. P. Incropera, Boiling heat transfer and critical heat flux in liquid films falling on vertically-mounted heat sources, *Int. J. Heat Mass Transfer* **30**, 2083–2095 (1987).
15. I. Mudawar and D. E. Maddox, Critical heat flux in subcooled flow boiling of fluorocarbon liquid on a simulated electronic chip in a vertical rectangular channel, *Int. J. Heat Mass Transfer* **32**, 379–394 (1989).
16. T. M. Anderson and I. Mudawar, Microelectronic cooling by enhanced pool boiling of a dielectric fluorocarbon liquid, *ASME J. Heat Transfer* **111**, 752–759 (1989).
17. D. Wadsworth and I. Mudawar, Cooling of a multichip electronic module by means of confined two-dimensional jets of dielectric liquid, *ASME J. Heat Transfer* **112**, 891–898 (1990).
18. W. H. McAdams, W. E. Kennel, C. S. Minden, C. Rudolf and J. E. Dow, Heat transfer at high rates to water with surface boiling, *Ind. Engng Chem.* **41**, 1945–1953 (1949).
19. A. E. Bergles and W. M. Rohsenow, The determination of forced convection surface-boiling heat transfer, *ASME J. Heat Transfer* **86**, 365–372 (1964).
20. R. Gardon and J. C. Akfirat, The role of turbulence in determining the heat-transfer characteristics of impinging jets, *Int. J. Heat Mass Transfer* **8**, 1261–1272 (1965).
21. Y. Katto and K. Ishii, Burnout in a high heat flux boiling system with a forced supply of liquid through a plane jet, *Proc. 6th Int. Heat Transfer Conf.*, Vol. 1, pp. 435–440 (1978).
22. Y. Katto and C. Kurata, Critical heat flux of saturated convective boiling on uniformly heated plates, *Int. J. Multiphase Flow* **6**, 575–582 (1980).
23. T. A. Grimley, I. Mudawar and F. P. Incropera, CHF enhancement in flowing fluorocarbon liquid films using structured surfaces and flow deflectors, *Int. J. Heat Mass Transfer* **31**, 55–65 (1988).

FLUX THERMIQUE CRITIQUE POUR UNE PUCE ELECTRONIQUE SIMULEE ET UN JET IMPACTANT CONFINE RECTANGULAIRE DE LIQUIDE DIELECTRIQUE

Résumé—Des expériences sont conduites pour étudier le transfert thermique par ébullition depuis une source de chaleur de 12,7 mm × 12,7 mm à un jet de liquide diélectrique Fluorinert FC-72 sortant d'un orifice rectangulaire mince et entrant dans un canal confiné entre les surfaces de la source de chaleur et la tuyère. Les tendances générales de l'ébullition et du flux thermique critique (CHF) sont examinées suivant les variations de la vitesse de sortie $U = 1$–13 m s^{-1}, de la largeur de la tuyère $W = 0{,}127$–$0{,}508$ mm et du sous-refroidissement $\Delta T_{sub} = 0$–40°C. Deux régimes de CHF, vitesses moyennes et élevées, sont découverts et une formule empirique est donnée pour le régime de vitesse moyenne. La différence principale entre les deux régimes est une faible dépendance du CHF vis-à-vis de la hauteur du canal pour les vitesses moyennes, ceci en opposition avec une forte dépendance pour les grandes vitesses. Un module comportant un arrangement 3 × 3 de sources de chaleur confirme l'uniformité et la prédicabilité du refroidissement de chacune des neuf sources thermiques, prouvant que la géométrie de jet confiné est bien cohérente pour les grands arrangements de sources thermiques à haute densité de puissance telles que des puces électroniques dissipant des densités de flux atteignant 250 W cm^{-2}.

KRITISCHE WÄRMESTROMDICHTE VON DER OBERFLÄCHE EINES SIMULIERTEN ELEKTRONISCHEN CHIP AN EINEN BEGRENZTEN RECHTECKIGEN STRAHL EINER DIELEKTRISCHEN FLÜSSIGKEIT

Zusammenfassung—Der Wärmeübergang von einer glatten Wärmequelle (12,7 mm × 12,7 mm) an einen Strahl aus flüssigem, dielektrischem Fluorinert FC-72 wird experimentell untersucht. Der Strahl tritt aus einer rechteckigen Öffnung in einen Kanal, der aus den Oberflächen der Wärmequelle und der Düse besteht. Die Abhängigkeit der Wärmestromdichte im allgemeinen sowie der kritischen Wärmestromdichte von der Strahlgeschwindigkeit im Düsenaustritt ($1 \leqslant U \leqslant 13$ m s^{-1}), vom Düsendurchmesser ($0{,}127 \leqslant W \leqslant 0{,}508$ mm), von der Höhe des Kanals über der beheizten Fläche ($0{,}508 \leqslant H \leqslant 5{,}08$ mm) und der Unterkühlung ($0 \leqslant \Delta T_{sub} \leqslant 40$°C) wird untersucht. Zwei Bereiche der kritischen Wärmestromdichte werden entdeckt: bei mittlerer und bei hoher Geschwindigkeit. Es wird eine empirische Korrelation für den mittleren Geschwindigkeitsbereich entwickelt. Der Hauptunterschied zwischen den beiden Bereichen ist die geringe Abhängigkeit der kritischen Wärmestromdichte von der Höhe des Kanals für mittlere Geschwindigkeiten, während bei hohen Geschwindigkeiten eine starke Abhängigkeit von der Kanalhöhe besteht. Es wird beobachtet, daß es bei hohen zunehmenden Geschwindigkeiten—insbesondere für die kleinste Kanalhöhe—zu einer Verringerung der kritischen Wärmestromdichte kommen kann. Dies ist eine Folge der Abnahme der Flüssigkeitsunterkühlung in Strömungsrichtung. Es werden zusätzliche Versuche mit einem getrennten Kühlmodul aus 3 × 3 Wärmequellen ausgeführt. Die Kühlung ist für sämtliche 9 Wärmequellen gleichmäßig und berechenbar. Dies beweist, daß die Anordnung mit begrenztem Strahl gut für die Kühlung großer Felder von Wärmequellen bei hoher Wärmestromdichte geeignet ist; dieses Problem tritt beispielsweise bei integrierten Schaltkreisen mit Verlustwärmestromdichten bis zu 250 W cm^{-2} auf.

КРИТИЧЕСКИЙ ТЕПЛОВОЙ ПОТОК ОТ МОДЕЛЬНОГО ЭЛЕКТРОННОГО ЧИПА К ОГРАНИЧЕННОЙ ПРЯМОУГОЛЬНОЙ ПАДАЮЩЕЙ СТРУЕ ДИЭЛЕКТРИЧЕСКОЙ ЖИДКОСТИ

Аннотация—Экспериментально исследуется теплоперенос в условиях кипения от гладкого источника тепла с размерами 12,7 × 12,7 мм к струе диэлектрической жидкости флуоринерт FC-72, истекающей из тонкого прямоугольного отверстия в канал, заключенный между поверхностями источника тепла и сопла. Общие тенденции развития процесса кипения и критического теплового потока (КТП) анализируются на основе изменений скорости на выходе из сопла, $U = 1$–13 м с$^{-1}$, ширины сопла $W = 0{,}127$–$0{,}508$ мм, высоты канала над нагретой поверхностью, $H = 0{,}508$–$5{,}08$ мм, а также недогрева $\Delta T_{sub} = 0$–40°C. Выявлено два режима КТП, а именно, со средней и высокой скоростями, и выведено обобщающее соотношение для режима средней скорости. Основное различие между двумя режимами состоит в слабой зависимости КТП от высоты канала при средних скоростях по сравнению с более сильной зависимостью от высоты канала при высоких скоростях. Найдено, что в случае режима высоких скоростей, особенно при минимальной высоте канала, КТП уменьшается с ростом скорости струи благодаря снижению недогрева жидкости в канале в направлении течения. Автономный модуль охлаждения, состоящий из набора тепловых источников 3 × 3, подтверждает равномерность и предсказуемость охлаждения каждого из девяти источников тепла и доказывает пригодность струи с конечной шириной для охлаждения больших наборов источников тепла с высокой плотностью энерговыделения, как, например, электронных чипов, которые рассеивают тепловые потоки величиной 250 Вт см$^{-2}$.